UC Irvine

Title

Discovery of a Gut Bacterial Metabolic Pathway that Drives α–Synuclein Aggregation

Permalink

https://escholarship.org/uc/item/3mm1r4nh

Journal

ACS Chemical Biology, 19(4)

ISSN

1554-8929

Authors

de Ora, Lizett Ortiz
Balsamo, Julia M
Uyeda, Kylie S
et al.

Publication Date

2024-04-19

DOI

10.1021/acschembio.4c00095

Supplemental Material

https://escholarship.org/uc/item/3mm1r4nh#supplemental

Copyright Information

Peer reviewed

Discovery of a Gut Bacterial Metabolic Pathway that Drives α-Synuclein Aggregation

Lizett Ortiz de Ora[1†], Julia M. Balsamo[1†], Kylie S. Uyeda[1], Elizabeth N. Bess[1,2]*

[1]Department of Chemistry, University of California, Irvine, California, USA 92617

[2]Department of Molecular Biology and Biochemistry, University of California, Irvine, California, USA 92617

[†]These authors contributed equally.

*Corresponding author: Elizabeth N. Bess, Departments of Chemistry and Molecular Biology & Biochemistry, University of California, Irvine, 1102 Natural Sciences II, Irvine, CA 92617, USA. E-mail: Elizabeth.Bess@uci.edu.

Abstract (250 words)

Parkinson's disease (PD) etiology is associated with aggregation and accumulation of α-synuclein (α-syn) proteins in midbrain dopaminergic neurons. Emerging evidence suggests that in certain subtypes of PD, α-syn aggregates originate in the gut and subsequently spread to the brain. However, the mechanisms that instigate α-syn aggregation in the gut have remained elusive. In the brain, the aggregation of α-syn is induced by oxidized dopamine. Such a mechanism has not been explored in the context of the gastrointestinal (GI) tract, a niche harboring 46% of the body's dopamine reservoirs. Here, we report that *Enterobacteriaceae*, a bacterial family prevalent in human gut microbiotas, induce α-syn aggregation. More specifically, our *in vitro* data indicate that respiration of nitrate by *Escherichia coli* K-12, which results in production of nitrite that mediates oxidation of Fe^{2+} to Fe^{3+}, creates an oxidizing redox potential. These oxidizing conditions enabled formation of dopamine-derived quinones and α-syn aggregates. Exposing nitrite, but not nitrate, to enteroendocrine STC-1 cells induced aggregation of α-syn that is natively expressed in these cells, which line the intestinal tract. Taken together, our findings indicate that bacterial nitrate reduction may be critical to initiating intestinal α-syn aggregation.

INTRODUCTION

Although Parkinson's disease (PD) has long been thought to originate in the brain, accumulating evidence indicates that some PD subtypes originate in the gastrointestinal (GI) tract.[1,2] PD is characterized by motor impairment that arises when α-synuclein (α-syn) protein aggregates accumulate in dopaminergic neurons of the substantia nigra, the brain site of motor control;[3] however, α-syn expression is not limited to the brain. α-syn is also expressed within the mucosa of the intestinal wall by enteroendocrine cells (EECs)[4] as well as by enteric neurons that innervate the GI tract.[5] At least eight years prior to onset of motor symptoms in people with idiopathic PD, α-syn aggregates accumulate in GI tissue.[6] These protein aggregates may subsequently propagate, putatively in a prion-like fashion, from the intestine to the brain via the vagus nerve that connects these organs.[7,8] While there is evidence that intestinal α-syn aggregates foreshadow neurodegeneration in the brain, the molecular-level mechanisms responsible for intestinal α-syn aggregation have remained poorly understood.

Several lines of evidence suggest a microbial component in the development of α-syn aggregates and progression of PD. The gut microbiota is distinct in people with PD as compared to non-diseased controls.[9–13] This dysbiosis is often characterized by an enrichment of the facultative anaerobic *Enterobacteriaceae* bacterial family whose abundance in the gut positively correlates with the severity of motor dysfunction in people with PD.[9,14–16] Although it remains controversial whether gut microbiota dysbiosis is a cause or a consequence of PD pathogenesis, studies using mouse models implicate the gut microbiome in the etiology of this disorder. In germ-free mice overexpressing α-syn, GI-tract colonization using fecal samples from people with PD exacerbated motor deficits and brain pathology as compared to colonization using fecal samples from non-diseased controls.[17] Additionally, induction of intestinal inflammation that is commonly associated with blooms in *Enterobacteriaceae* (DSS-induced colitis)[18,19] resulted in accumulation of α-syn in GI tracts followed by the pathogenic buildup of this protein in the brains of α-syn-overexpressing mice.[20,21]

To identify specific gut bacterial biochemical processes that induce α-syn aggregation in the GI tract, we sought clues in characterized mechanisms of α-syn aggregation in the brain. In brain dopaminergic neurons, iron and dopamine can form a toxic pair that leads to aggregation of neural α-syn

(Figure 1). Aging-related accumulation of iron in dopaminergic neurons causes oxidative stress that results in labile cytosolic ferrous iron (Fe^{2+}) being oxidized to ferric iron (Fe^{3+}).[22] Cytoplasmic dopamine that is abundant in dopaminergic neurons can be readily oxidized by Fe^{3+} to highly reactive *ortho*-quinones.[23] Dopamine-derived quinones interact with neural α-syn to cause misfolding that results in toxic α-syn oligomers.[24]

Like in the brain, the GI tract harbors dopamine and iron as well as expresses α-syn. Of the body's dopamine pool, 46% is contained in the GI tract,[25] and the gut microbiota is responsible for elevating the dopamine concentration in intestinal tissue.[26] Iron, which can mediate dopamine oxidation, is present in high concentrations in the intestinal lumen (up to 25 mM), and increased dietary iron increases iron levels in intestinal cells.[27] Although the oxidation state of labile cytosolic iron is predominantly Fe^{2+} in the non-diseased GI tract,[28] conditions of oxidative stress increase the concentration of Fe^{3+}, which could oxidize dopamine as depicted in Figure 1. With the convergence of concentrated dopamine and iron in the intestinal epithelium as well as the expression of α-syn by intestinal EECs and enteric neurons, α-syn aggregation is poised to occur in the GI tract. We sought to identify gut bacterial biochemical processes that supply an oxidant capable of inducing iron-mediated dopamine oxidation and subsequent α-syn aggregation.

Although changes in redox potential that induce oxidative stress in the GI tract are typically associated with host metabolic processes,[29–33] gut bacteria also modulate the redox potential of their environment.[34] Here, we describe that the ability of *Escherichia coli* (a prototypic gut bacterium of the *Enterobacteriaceae* bacterial family[18]) to create an environment with an oxidizing redox potential is a stimulus that provokes iron and dopamine to cause α-syn aggregation. We identify that nitrite, which is an oxidant generated during *Enterobacteriaceae* nitrate dissimilatory metabolism that mediates oxidation of Fe^{2+} to Fe^{3+} in bacteria,[18,35–37] stimulates a cascade of oxidation reactions that results in α-syn aggregation. Our results from *in vitro* experiments with both bacterial cultures and α-syn-expressing intestinal epithelial cells suggest a novel molecular mechanism by which the gut microbiota may influence PD pathogenesis.

RESULTS

E. coli nitrate respiration creates an environment of oxidizing redox potential.

Given the positive correlation between PD severity and the abundance of *Enterobacteriaceae* in the gut microbiotas of people with PD,[9] we sought to determine whether metabolic capabilities of this bacterial family are implicated in the pathogenic aggregation of α-syn. We were particularly intrigued by *Enterobacteriaceae*'s ability to perform anaerobic nitrate respiration, which results in production of an oxidant, nitrite.[18,38,39] We hypothesized that an oxidizing redox potential would be created by nitrate-respiring *Enterobacteriaceae* and, thereby, stimulate shifts in the relative abundance of labile iron from being mainly Fe^{2+} (which putatively predominates in the reducing conditions of the gut microbiota[40]) to Fe^{3+} (which could subsequently oxidize dopamine and induce α-syn misfolding and aggregation).

To test our hypothesis, we anaerobically cultured *Escherichia coli* K-12 to enable two types of metabolism: fermentation and respiration. Fermentation conditions were created by culturing *E. coli* K-12 in a minimal-nutrient medium supplemented with Fe^{2+} (500 µM) as well as glucose (20 mM) as the sole carbon source but without nitrate (media referred to as $mM9_{-NO3}$). Conditions for nitrate respiration were generated by supplementing the same medium with nitrate (50 mM; media referred to as $mM9_{+NO3}$). As shown in Figure 2a, supplementation with nitrate afforded a 1.6-fold increase in bacterial growth after 12 hours of incubation as measured by optical density of cultures at 600 nm (OD_{600}). These findings are consistent with reported *in vivo* findings: due to nitrate respiration being more energetically lucrative than fermentative metabolism,[41] a higher concentration of intestinal nitrate enables a bloom in *Enterobacteriaceae* abundance in the gut microbiota.[18]

In *E. coli* K-12 cultures, we also evaluated fluctuations in redox potential as a function of bacterial metabolism. A reducing redox potential (relative to sterile controls) was observed when bacteria was cultured in $mM9_{-NO3}$ (Figure 2b). The progressively more reducing redox potential observed over the course of exponential bacterial growth is characteristic of fermentative metabolism that yields hydrogen, a reducing agent.[42] In contrast, bacteria cultured in $mM9_{+NO3}$ demonstrated a steadily increasing oxidizing redox potential (relative to sterile controls) over 18 hours of incubation, reaching a maximum value of 308.17±7.62 mV (Figure 2b). Notably, increases in oxidative redox potential mirrored accumulation of nitrite in culture media (Figure 2c). Further supporting nitrite's role as a redox-active metabolite, we

observed that supplementation of sodium nitrite to sterile mM9 medium (mM9$_{+NO2}$) afforded increases in redox potential in a concentration dependent manner (Figure S1). In contrast, uninoculated sterile media supplemented with sodium nitrate (mM9$_{+NO3}$) showed no significant variation in the redox potential of the solution. These findings support the notion that bacterial nitrate respiration can shift the redox potential of the environment to being more oxidizing through the production of nitrite.

We next assessed whether the oxidizing redox potential afforded by nitrate-respiring conditions could shift the balance of iron speciation from favoring Fe^{2+} to favoring Fe^{3+}. *E. coli* K-12 was cultured in mM9$_{-NO3}$ or mM9$_{+NO3}$ media, and the relative abundance of Fe^{2+} and Fe^{3+} was measured using the ferrozine assay.[43] Under fermentation conditions that afforded a reducing redox potential (mM9$_{-NO3}$), Fe^{2+} was the predominant iron species (Figure 2d). Conversely, in culture conditions for bacterial nitrate respiration (mM9$_{+NO3}$), the oxidizing redox potential that corresponded to production of nitrite drove iron oxidation such that Fe^{3+} became the dominant oxidation state of iron (Figure 2e). Taken together, these findings demonstrate that the presence of nitrate enhances *E. coli* K-12 growth as well as creates an oxidizing redox potential that corresponds to nitrite production and that results in the predominance of Fe^{3+} over Fe^{2+} in culture media.

E. coli nitrate respiration initiates a cascade of oxidation reactions that lead to α-syn aggregation.

Next, we sought to determine whether bacterial nitrate respiration could incite the cascade of oxidation reactions that are implicated in dopamine-dependent α-syn aggregation in cerebral dopaminergic neurons but that remain unexplored in the GI tract: Fe^{3+}-mediated dopamine oxidation that forms *ortho*-quinones[44–46] that cause α-syn to misfold and, subsequently, aggregate.[23,24] To this end, we again anaerobically cultured *E. coli* K-12 until stationary phase (14 hours) in either mM9$_{+NO3}$ or mM9$_{-NO3}$ but with the addition of α-syn monomer (20 μM) as well as dopamine (500 μM; mM9$_{+NO3,+DA}$ or mM9$_{-NO3,+DA}$, respectively) or its vehicle (mM9$_{+NO3,-DA}$ or mM9$_{-NO3,-DA}$, respectively). As before, bacteria cultured in nitrate-respiring conditions reduced nitrate to nitrite (Figure 3a). Accumulation of nitrite corresponded to an oxidizing redox potential (Figure 3b) and a shift in iron speciation so that the relative abundance of Fe^{3+} increased in comparison to cultures without nitrate supplementation (Figure 3c).

Culture conditions in which nitrite was produced and dopamine was also present resulted in lower relative abundance of Fe^{3+} as compared to conditions without dopamine. This finding is putatively a reflection of dopamine oxidation being coupled to reduction of Fe^{3+}, thereby increasing the relative abundance of Fe^{2+}. Correspondingly, we were not able to measure redox potential in culture conditions that contained dopamine, as redox potential did not stabilize under these conditions.

In cultures containing dopamine, we observed formation of a dark pigment, which is characteristic of quinones (Figure 3d).[47] Redox-cycling stain nitroblue tetrazolium (NBT), which specifically stains quinones,[48] enabled detection of quinones in dot blots of nitrate-reducing bacterial cultures (Figure 3e and Figure S2). Contrastingly, and as depicted in Figure 3d, no dark pigment was observed in dopamine-supplemented fermentative culture conditions (mM9$_{-NO3,+DA}$) wherein Fe^{3+} relative abundance was significantly less than in respiration culture conditions (mM9$_{+NO3,+DA}$); correspondingly, no quinones were detected by NBT stain (Figure 3e; positive control shown in Figure S2). In the absence of dopamine supplementation to culture media, quinones were neither detected in nitrate-reducing nor in fermenting bacterial cultures. These data indicate that dopamine supplementation is necessary for quinone formation and that dopamine-dependent quinone formation occurs in the oxidizing conditions created upon bacterial reduction of nitrate.

Strikingly, dopamine-dependent quinone formation coincided with α-syn aggregation. Evaluation of α-syn aggregation was conducted by dot blot, immunostaining α-syn aggregates using antibody MJFR-14 on membranes spotted with culture media (Figure 3f; positive control shown in Figure S3). Significantly greater amounts of α-syn aggregates formed in nitrate-reducing conditions as compared to fermentative conditions—but only when dopamine was present (Figure 3g and Figure S3). In the absence of dopamine, a culture environment of oxidizing redox potential (mM9$_{+NO3,-DA}$; Figure 3b) was not sufficient to induce α-syn aggregation (Figure 3g and Figure S3). Nitrite-induced dopamine-dependent α-syn aggregation was recapitulated in abiotic experiments in which nitrite was exogenously supplied, rather than produced by bacteria (Figure S4). This finding was consistent irrespective of the antibody used for detection: either MJFR-14 or 5G4, with the latter displaying enhanced selectivity for detecting α-syn aggregates relative to monomers (Figure S5).

We next used a genetic knockout of nitrate respiration to further clarify the roles of nitrate and nitrite in initiating α-syn aggregation. First, we targeted a molybdenum cofactor (MoaA) that is incorporated in the active site of nitrate reductases and is essential for this enzyme to reduce nitrate to nitrite.[49] MoaA was deleted from *E. coli* K-12 wild-type to create the isogenic mutant *E. coli* K-12 Δ*moaA*. Culturing *E. coli* K-12 Δ*moaA* in mM9$_{+NO3}$ media did not afford the growth advantage that was obtained when, upon culturing in the same media, *E. coli* K-12 wild-type performed nitrate reduction (Figure S6). Moreover, *E. coli* K-12 Δ*moaA* did not produce redox-active nitrite (Figure 3a), indicating that nitrate reduction was, indeed, inhibited by genetic deletion of *moaA*; likewise, a significantly less oxidizing redox potential was observed as compared to cultures of the wild-type strain cultured in mM9$_{+NO3}$ media (Figure 3b). The less oxidizing redox potential of *E. coli* K-12 Δ*moaA* cultures corresponded to significant reductions in the relative abundance of Fe^{3+} when *E. coli* K-12 Δ*moaA* was cultured in either mM9$_{+NO3,-DA}$ or mM9$_{+NO3,+DA}$ as compared to analogous cultures of *E. coli* K-12 wild-type (Figure 3c). Without the ability of *E. coli* K-12 Δ*moaA* to reduce nitrate and increase the oxidizing redox potential of the culture media, neither dopamine oxidation nor α-syn aggregation occurred (Figures 3e, 3f, 3g; Figures S2 and S3). Taken together, these data indicate that the presence of nitrate, alone, does not induce α-syn aggregation; instead, we have demonstrated that bacteria that produce nitrite can transform an innocuous trio—Fe^{2+}, dopamine, and α-syn monomers—into one that generates toxic α-syn aggregates.

Tungstate inhibits α-syn aggregation induced by bacterial nitrate reduction.

After identifying the instigating role of bacterial reduction of nitrate to nitrite in α-syn aggregation, we were curious about whether α-syn aggregation could be mitigated by chemically inhibiting bacterial nitrate respiration. To this end, we turned to tungstate, a chemical analog of molybdate that renders *Enterobacteriaceae* nitrate reductases inactive.[19] We evaluated the effect of sodium tungstate (0.5–100 mM) on *E. coli* K-12 (wild-type and Δ*moaA*) cultured until stationary phase (14 hours) in mM9$_{+NO3}$ media supplemented with α-syn monomer (20 μM) and with or without dopamine (Figure S7). For *E. coli* K-12 wild-type cultures, a dose-response relationship was observed: increasing concentrations of sodium tungstate resulted in decreasing production of nitrite (Figure 4a).

In accordance with our findings that bacterial reduction of nitrate to nitrite creates a more oxidizing redox potential, progressive inhibition of this process using increasing concentrations of sodium tungstate supplemented to cultures of *E. coli* K-12 wild-type (in the absence of dopamine) correlated with decreasing oxidizing redox potentials of cultures (Figure 4b). As the redox potential of *E. coli* K-12 wild-type cultures decreased with increasing concentrations of tungstate, the relative abundance of Fe^{3+} also decreased in cultures with dopamine (Figure 4c) and without dopamine (Figure 4d). Tungstate (0.5–50 mM) inhibition of nitrate reduction by *E. coli* K-12 wild-type corresponded with decreased visible pigmentation of cultures (Figure 4e) and NBT-stained quinone (Figure 4f and Figure S2) as well as decreased formation of α-syn aggregates (Figures 4g and 4h; Figure S3). Although increasing tungstate concentrations from 0.5 mM to 100 mM resulted in significantly decreased nitrite level, relative redox potential, Fe^{3+} relative abundance, and α-syn aggregation, supplying *E. coli* K-12 wild-type cultures with up to 100 mM of tungstate did not ameliorate the effects of nitrite reduction to the extent that was observed upon genetic deletion of *moaA*. With 100 mM tungstate, nitrite concentration, Fe^{3+} relative abundance, and α-syn aggregates remained significantly greater in cultures of *E. coli* K-12 wild-type as compared with *E. coli* K-12 Δ*moaA*. Taken together, these results indicate that tungstate is a means to chemically limit (but not fully prevent) generation of the oxidizing environment created by *E. coli* nitrate reduction and, thereby, inhibit the cascade of oxidation reactions that lead to α-syn aggregation.

Redox-active nitrite induces α-syn aggregation in specialized gut epithelial cells.

We next set out to examine the relevance of our proposed bacteria-induced α-syn aggregation mechanism to the mammalian gut. In the GI tract, α-syn is expressed by specialized epithelial cells called enteroendocrine cells (EECs);[4] the dopamine metabolic pathway is also expressed by these cells.[50] EECs are chemosensory cells at the interface between gut luminal contents and the nervous system. While the apical side of these cells is in direct contact with the gut microbiome and its metabolites, a cellular projection (called a neuropod) on the basolateral surface of EECs forms synapses with enteric neurons, including those of the vagus nerve.[51] Thus, EECs have been proposed as a potential site where

environmental factors, including bacterial metabolites, could initiate α-syn misfolding and the prion-like cascade leading to PD.[4,52]

Owing to gut epithelial cells absorbing nitrite through passive diffusion,[53] we hypothesized that this redox-active metabolite that is produced in the gut lumen by nitrate-respiring bacteria[18,19] could induce aggregation of α-syn that is present in the cytoplasm of EECs.[4] To test our hypothesis, we used murine STC-1 cells, an accepted model cell line for elucidating properties of native EECs.[54] STC-1 cells were incubated with nitrate or nitrite (0.05–50 mM), and α-syn aggregation was analyzed via immunofluorescence staining using an antibody for α-syn fibrils (Figure 5a). STC-1 cells treated with 0.5 mM nitrate as compared to untreated cells showed no significant difference in amounts of α-syn aggregates (Figure 5b). In contrast, treatment with nitrite significantly induced α-syn aggregation in a concentration dependent manner, with 0.5 mM, 5 mM, and 50 mM nitrite resulting in 2.1-, 12.9-, and 77.0-fold increases in aggregation, respectively, as compared to nitrate-treated cells (Figure 5b). Supplying cells with 0.05 mM nitrite afforded no significant amount of α-syn aggregation as compared to nitrate-treated cells. Staining cells with an isotype control demonstrated no significant non-specific background interactions (Figure S8). Taken together, these results not only provide strong evidence for our proposed model that nitrite induces α-syn aggregation within intestinal cells expressing this protein, but these findings also emphasize the importance of bacterial reduction of nitrate to nitrite to incite this pathogenic process.

DISCUSSION

Here, we show that the ability of *Enterobacteriaceae*, specifically *E. coli*, to modulate the redox potential of a bacterium's environment plays a critical role in inducing the formation of α-syn aggregates. Microbial metabolism has been previously demonstrated to influence the redox potential of the environment;[34] however, gut bacterial metabolic pathways are typically associated with creating more reducing environments, while the generation of oxidizing environments is commonly linked to host processes.[29–33,55] Our data suggest that bacteria performing nitrate dissimilatory metabolism can generate an oxidizing environment. When this metabolic process occurs, *Enterobacteriaceae* reduce

nitrate, a relatively redox-inert by-product of the host inflammatory response,[56] to nitrite, an oxidizing agent.

Using *E. coli* K-12 wild-type cultures, we demonstrated that the presence of nitrate in the growth medium results in its reduction to nitrite as well as a generation of a redox environment that is more oxidizing as compared to the same cultures without nitrate. In contrast, nitrate supplied to bacteria with a nitrate respiration defect (i.e., *E. coli* K-12 Δ*moaA*) or to sterile media neither resulted in nitrite production nor a more oxidizing redox potential. These data indicate that *E. coli* K-12 nitrate metabolism generates an oxidizing environment. Notably, we showed that the shift in redox potential that accompanies nitrite production was sufficient to alter the relative abundance of iron species so that Fe^{3+} predominated over Fe^{2+} in cultures. This shift occurred in spite of anaerobic and reducing *in vitro* culture conditions similar to those of the GI tract that favor the prevalence of Fe^{2+} over Fe^{3+}.[40] *Enterobacteriaceae* nitrate respiration may be an underappreciated mechanism by which gut bacteria disrupt their environment's relative abundance of Fe^{2+} and Fe^{3+} as well as the metabolic processes mediated by this redox-active metal.

Iron has been implicated in PD onset due to the ability of Fe^{3+} to oxidize dopamine to *ortho*-quinones that cause α-syn monomers to aggregate.[24,57,58] Through *in vitro* experiments, we demonstrated that gut bacterial nitrate reduction can induce the cascade of oxidation reactions that ultimately results in dopamine-dependent α-syn aggregation. This is the first report elucidating a gut bacterial metabolic pathway that directly influences α-syn aggregation *in vitro*. If conserved in the mammalian GI tract, this biochemical pathway may be a novel target for intervention strategies to prevent α-syn aggregation in the gut.

Due to tungstate's inhibition of *Enterobacteriaceae* nitrate respiration,[19] we sought to determine whether tungstate could be used to inhibit *Enterobacteriaceae*-induced α-syn aggregation. Tungstate exposure limited dopamine oxidation and α-syn aggregation in cultures of *E. coli* K-12 wild-type supplemented with nitrate. Additionally, tungstate treatment effectively lessened the oxidizing redox potential of the bacterial environment as well as increased the relative abundance of less-oxidizing Fe^{2+}. Owing to the ability of oral tungstate treatment to effectively ameliorate murine colitis, which is

exacerbated by gut bacterial nitrate respiration,[19] the ability of tungstate to limit α-syn aggregation *in vitro* may have important therapeutic implications for limiting α-syn aggregation in the mammalian intestine.

Towards determining the significance of bacterial nitrate respiration to α-syn aggregation in the gut, we focused our efforts on EECs. EECs are emerging as a critical mediator of the gut–brain axis[59,60] and have been implicated in PD as a source of intestinal α-syn.[4,52] Since EECs can form synapses with the enteric nervous system,[59] it has been hypothesized that α-syn aggregates may spread from EECs to the brain via the vagus nerve;[4,52] however, the precise molecular stimuli of α-syn aggregation in EECs have remained elusive. Owing to our findings that nitrite induces dopamine-dependent α-syn aggregation *in vitro*, we suspected that nitrite could induce the same process in EECs. Within EECs, nitrite exposure (0.5–50 mM) afforded a dose-dependent increase in the amount of α-syn aggregation. Consistent with our *in vitro* experiments, the effect of nitrate (0.5 mM) on α-syn aggregation was no different than sham treatment. Notably, the concentration of nitrate in the mucus layer of the intestinal lumen is on the order of 0.5 mM,[18] which supports the physiological relevance of our findings. We demonstrated that nitrite—the product of gut bacterial *Enterobacteriaceae* nitrate respiration that occurs within the GI tract[18,19]—can induce α-syn aggregation in EECs, which line the GI lumen.

In summary, our data demonstrate that the gut microbiota, in particular *E. coli* (a prototypic organism of the *Enterobacteriaceae* bacterial family[18]), is capable of inducing α-syn aggregation. *Enterobacteriaceae* are more abundant in people with PD as compared to non-diseased, age-matched controls and are positively correlated with the severity of motor dysfunction;[9] however, whether *Enterobacteriaceae* plays a causative role in PD has remained unknown. Here, we identified a specific metabolic pathway, bacterial nitrate reduction, by which *Enterobacteriacaeae* can generate the oxidative environment that causes dopamine oxidation and subsequent α-syn aggregation (working model depicted in Figure S9). While dopamine oxidation has been identified as a crucial component of α-syn aggregation mechanisms in the brain,[24,57,58] we have demonstrated that dopamine-dependent mechanisms of α-syn aggregation are also likely relevant in the gut. Our findings that nitrite induces α-syn aggregation in EECs provides strong motivation for examining these cells as a likely conduit of the gut–brain axis in PD. Future work will focus on the ability of α-syn aggregates to spread to the enteric

nervous system following their formation in EECs. If the cascade of reactions initiated by bacterial nitrate reduction and ending with α-syn aggregation is conserved in the mammalian gut, our findings position gut bacterial nitrate reduction as a novel target that may be leveraged for early intervention strategies to prevent intestinal α-syn aggregation and limit Parkinsonian neurodegeneration.

MATERIALS AND METHODS

Bacteria and culture conditions

General

Escherichia coli K-12 BW25113 was acquired from VWR (470179-082). *Escherichia coli ΔmoaA* was constructed as previously described.[61,62] Archived stocks of bacteria were maintained in 16% glycerol at -80 °C. Bacteria were routinely cultured in modified M9 mineral media (mM9, defined below) at 37 °C under anoxic and reducing conditions (2–5% H_2, 20% CO_2, with the balance being N_2) in a COY anaerobic chamber. When indicated, mM9 media (described below) was supplemented with 50 mM sodium nitrate (Sigma, S5506-250G), 50 mM sodium nitrite (Fisher Scientific, M1065490100), 500 µM dopamine HCl (Alfa Aesar, A11136-06) and/or 20 µM α-synuclein (purified as described below). Prior to beginning experiments, media was equilibrated in anoxic conditions overnight to remove oxygen.

mM9 media was prepared to contain the following: 1x M9 salts (Sigma, M6030-1KG), 2 mM magnesium sulfate (Fisher Scientific, 0338-500G), 100 µM calcium chloride (Fisher Scientific, AC219171000), 20 mM D-glucose anhydrous (VWR Life Science, Biotechnology Grade), 0.2% (*w/v*) casamino acids (Fisher Scientific, DF0288-15-6), 1x vitamin supplement (ATCC, MD-VS), and 500 µM ferrous iron chloride (Oakwood, 098678-5g).

Purification of recombinant α-synuclein

Purification of α-synuclein was performed according to the method of Huang et al., 2005.[63] Briefly, an overnight culture of *E. coli* Rosetta 2 transformed with pET-21a-α-synuclein (Addgene, 51485*)* was diluted 100-fold in LB supplemented with 100 µg/mL ampicillin. Expression of α-synuclein was induced for 5 hours by adding 100 µM IPTG to the culture media when cell density reached an OD_{600} of 0.3–0.4.

The cell pellet from a 1 L culture was resuspended in 100 mL of osmotic shock buffer (30 mM Tris–HCl, 40% sucrose, and 2 mM ethylenediaminetetraacetic acid disodium, pH 7.2) and incubated for 10 minutes at room temperature. The pellet collected by centrifugation at 12,000 rpm for 20 min was quickly resuspended in 90 mL of cold water followed by adding 37.5 µL of saturated $MgCl_2$. The resuspension was kept on ice for 3 min. The supernatant containing periplasm proteins was collected by centrifugation at 3500 x g for 20 min and dialyzed overnight against buffer A (20 mM Tris–HCl, pH 8.0). After centrifugation at 3500 x g for 20 min, the supernatant was loaded onto a DEAE Sepharose column (GE healthcare) and eluted with a 0–0.5 M NaCl gradient in buffer A. The elution fractions were analyzed by SDS–15% PAGE, and the fractions containing only an 18 kDa band were combined for size-exclusion chromatography in 0.0095% $MgCl_2$, 0.316% Tris–HCl, 0.58% NaCl, pH 7.5. Fractions containing pure α-synuclein were concentrated to 1 mg/mL, aliquoted, and stored at -20 °C.

Redox potential measurements

Redox potential was measured in 5 mL bacterial cultures using a redox electrode with an Ag/AgCl reference electrode (Cole-Parmer, EW-59001-75). The values are reported relative to the standard hydrogen electrode (SHE) and were determined by measuring the offset of the reference electrode in a reference solution with a known redox potential (Thermo Scientific, 967961). Relative oxidation-reduction potential (ORP) was determined by subtracting the ORP value of the sterile control from the ORP of experimental conditions.

Nitrate and nitrite measurements

To determine nitrate concentrations, the Griess-vanadium chloride method developed by Miranda *et al.* was used, with slight modifications.[64] Briefly, 2 µL of bacterial culture was diluted in 198 µL of 1 M HCl. Of this suspension, 50 µL were mixed with 50 µL of a solution containing 0.1 % (*w/v*) sulfanilamide (Sigma, S9251-100G) and 0.05% (*w/v*) *N*-(1-naphthyl)ethylenediamine dihydrochloride (Sigma, N9125-10G) in 0.5 M HCl followed by the rapid addition of 50 µL of 0.25 % (*w/v*) vanadium (III) chloride (Sigma, 208272-1G) in 1 M HCl. The mixture was incubated at 37 °C for 30 minutes. Nitrite was evaluated in a

similar manner except that samples were exposed to 50 μL of 1 M HCl instead of vanadium (III) chloride. In either case, following incubation the absorbance at 540 nm was measured using a SPECTROstar Nano plate reader (BMG LABTECH). Sample concentrations were determined using calibration curves generated by measuring absorbance at 540 nm and performing linear regression against known concentrations of nitrate and nitrite prepared from sodium nitrate or sodium nitrite standards, respectively, at concentrations ranging from 1000 to 15.62 μM (2-fold dilution series).

Iron speciation assay

To determine the ratio of Fe^{2+}/Fe^{3+} in media, we used the Fe^{2+}-ferrozine assay as previously described, with slight modifications.[43] Briefly, to determine the concentration of Fe^{2+} present in media, bacterial culture (70 μL) was mixed with 70 μL of 50 mg/mL ferrozine (Hach, 230424) in 1 M potassium acetate buffer (pH 5.5). To determine total iron present in the solution, ascorbic acid was used as a reducing agent to reduce Fe^{3+} to Fe^{2+}. For this purpose, bacterial culture (90 μL) was mixed with 100 μL of 50 mg/mL ferrozine in 1 M potassium acetate buffer (pH 5.5) and 10 μL of 1 M ascorbic acid (Sigma, A92902-25G). Reduced and non-reduced samples were incubated at 37 °C for 30 minutes followed by centrifugation at 3000 x *g* for 15 minutes. Then, 100 μL of supernatant was used to determine the light absorption of Fe^{2+}-ferrozine complex at 562 nm using a SPECTROstar Nano plate reader (BMG LABTECH). Sample concentrations were determined using calibration curves generated by measuring absorbance at 562 nm and performing linear regression against known concentrations of Fe^{2+} prepared from $FeCl_2$ standards at concentrations ranging from 100 to 1.56 mM (2-fold dilution series). Fe^{3+} was calculated as the difference between total iron (the sum of Fe^{2+} and Fe^{3+} reduced to Fe^{2+}) and Fe^{2+}.

Nitroblue tetrazolium assay for the detection of quinones

The presence of quinones in bacterial cultures was evaluated as previously described.[48] Briefly, under ambient conditions, 2 μL of each sample was spotted onto a polyvinylidene difluoride (PVDF) membrane (Fisher Scientific, ISEQ00005) that was previously activated in methanol and equilibrated in tris-buffered saline (pH 7.4). As a positive control, 2 μL of oxidized dopamine produced by *Aspergillus*

tyrosinase (Worthington Biochemical, LS003789; detailed protocol described below) was used. The membrane was left to dry for at least one hour. Then, the membrane was reactivated using methanol and submerged in a solution of 0.6 mg/mL nitroblue tetrazolium (Santa Cruz Biotechnology, sc-296003) in a potassium glycinate buffer (pH 10). The membrane was then incubated at room temperature, in the dark, for 45 minutes. After incubation, the membrane was washed twice in a solution of 0.16 M sodium borate (Sigma, S9640-25G) and photographed using an Epson V19 scanner.

Dopamine oxidation using tyrosinase

Lyophilized *Aspergillus* tyrosinase (Worthington Biochemical, LS003789) was resuspended in 1000 µL 50 mM phosphate buffer, 15% glycerol, pH 6.5, to create a 24 kU/mL solution (50 mg/mL, 390 µM). Single-use aliquots (100 µL) were prepared and stored at -20 °C. Aliquots were thawed on ice shortly before use. Dopamine (500 µM) was oxidized by adding 250 U (3.9 µM) of tyrosinase. The solution was incubated for one hour at room temperature.

Immunodetection of α-synuclein aggregates

α-Syn aggregation was evaluated in methanol-activated PVDF membranes. Under anaerobic conditions, 2 µL of bacterial cultures were spotted and left to dry for at least one hour. As controls, 2 µL of monomeric (Abcam, ab51189) and aggregated α-synuclein (Abcam, ab218817) were each spotted into the membrane. The membrane was immunostained with anti-fibril α-synuclein (Abcam, ab209538; 1:50,000 dilution) as primary antibody and NIR 800CW donkey anti-rabbit IgG secondary antibody (LI-COR, 926-32213) according to the manufacturer's instructions. The membranes were visualized using an Odyssey CLx imager (LI-COR) using the 800 nm channel. α-syn aggregates were quantified using Image studio data analysis software (LI-COR). Relative fluorescence units (R.F.U.) values were scaled relative to sterile control samples, which were set equal to zero.

Abiotic incubations

Samples with sodium nitrate (50 mM; Sigma), sodium nitrite (50 mM; Fisher Scientific), dopamine HCl (500 µM; Alfa Aesar), ferrous iron chloride (500 µM; Oakwood), and/or recombinant human α-syn monomer (20 µM; Abcam, ab51189) in double-deionized water (36 µL) were prepared in anoxic and reducing conditions (2–5% H2, 20% CO_2, with the balance being N_2) in a COY anaerobic chamber. Samples were aliquoted into three 12-µL volumes. These triplicates were then incubated, in PCR tubes, at 37 °C for 4 hours in the anaerobic chamber described.

Immunodetection of α-synuclein aggregates

α-syn aggregation was evaluated in methanol-activated PVDF membranes. Under anaerobic conditions, 2 µL of each sample was spotted onto three different methanol-activated PVDF membranes. As controls, 2 µL (578 ng) of monomeric α-syn (Abcam, ab51189) and 578 ng of aggregated α-syn (Abcam, ab218817) were spotted onto each membrane. The membranes were allowed to dry for 1 h. One membrane was used as a quantitative control to ensure the protein concentration in each sample was equivalent. The dried membrane was washed with DDI water before submerging it in Ponceau stain, which had been prepared to contain Ponceau S (Sigma-Aldrich) and glacial acetic acid (Fisher Scientific). Ponceau stain was discarded after 1 min, and the membrane was subsequently washed with DDI water to remove excess before visualizing. The other two membranes were blocked for 1 h using 5% Blotting Grade Blocker Non-Fat Dry Milk (Bio-Rad) in TBS. One of the blocked membranes was then probed with the MJFR-14 anti-aggregate α-syn primary antibody (Abcam, ab209538; 1:10000 dilution) for 2 h before being incubated overnight at 4 °C. After four 5-min washes with TBS-T (0.1% Tween 20 (Sigma-Aldrich) in the prepared TBS), the membrane was subsequently immunostained with IRDye 800CW donkey anti-rabbit IgG secondary antibody (LI-COR, 926-32213; 1:20000 dilution) for 45 min in the dark. Four more washes using TBS-T followed, before rinsing off the Tween 20 with TBS. The other blocked membrane was immunostained with the 5G4 anti-aggregate primary antibody (Millipore Sigma, MABN389; 1:4000 dilution) and IRDye 800CW donkey anti-mouse IgG secondary antibody (LI-COR, 926-32212; 1:20000 dilution). The same steps as described above were followed for washing and immunostaining with the secondary antibody. The membranes were visualized using an Odyssey CLx imager (LI-COR) on the

800 nm channel. Blots were quantified using Image Studio data analysis software (LI-COR) to analyze relative aggregation of α-syn. Prism was used for further data processing.

Antibody selectivity for α-synuclein aggregate versus monomer

In double-deionized water, α-syn monomer (1 mg/mL; Abcam, ab51189) and α-syn aggregate (2 mg/mL; Abcam, ab218817) were each used to prepare separate dilution series containing the following amounts of protein: 350 ng/μL, 289 ng/μL, 144.5 ng/μL, 72.3 ng/μL, 36.1 ng/μL, 18.1 ng/μL, 9.03 ng/μL. Of each sample, 2 μL was spotted in duplicate onto two different methanol-activated PVDF membranes, affording the following amounts of α-syn monomer or α-syn aggregate on the membranes in each dot: 700 ng, 578 ng, 289 ng, 144 ng, 72.3 ng, 36.1 ng, 18.1 ng. Using the procedures described above, one membrane was immunostained using MJFR-14 anti-aggregate α-syn primary antibody (Abcam, ab209538; 1:10000 dilution) followed by IRDye 800CW donkey anti-rabbit IgG secondary antibody (LI-COR, 926-32213; 1:20000 dilution). The other membrane was immunostained using 5G4 anti-aggregate primary antibody (Millipore Sigma, MABN389; 1:4000 dilution) and IRDye 800CW donkey anti-mouse IgG secondary antibody (LI-COR, 926-32212; 1:20000 dilution). The membranes were visualized using an Odyssey CLx imager (LI-COR) on the 800 nm channel. Blots were quantified using Image Studio data analysis software (LI-COR) to analyze relative aggregation of α-syn. Prism was used for further data processing.

Cell lines and growth conditions

General

Enteroendocrine STC-1 (CRL-3254) cell line was obtained from the American Type Culture Collection (ATCC). Cells were cultured in Dulbecco's Modified Eagle Medium (DMEM, Corning) containing 4.5 g/L glucose, 2 mM L-glutamine, 10% (v/v) fetal bovine serum (Life Technologies), penicillin (100 U/mL), and streptomycin (100 μg/mL, Gibco). Cells were incubated at 37 °C in a humidified atmosphere containing 5% CO_2. Cells were serially passaged using 0.25% Trypsin-EDTA (Gibco). Cells were seeded onto two 8-well glass slides (Ibidi) at a density of 1×10^5 viable cells/well and incubated for

48 hours. Then, the growth media was replaced with fresh media supplemented with either sodium nitrate, sodium nitrite, or vehicle. Cells were incubated for another 24 hours before fixation.

Immunofluorescence

Fixation was performed using 10% formalin (Fisher Scientific, 22-170-402) for 20 minutes at room temperature. Cells were then permeabilized for another 20 minutes at room temperature using 0.1% Triton X-100 (Bio-Rad, 1610407) in phosphate-buffered saline (PBS), pH 7.4. After discarding the permeabilization solution, wells were washed with PBS, twice. Samples were then blocked for 1 hour at room temperature in PBS containing 5% Normal Goat Serum (Thermo Scientific, 50197Z) and 0.2% bovine serum albumin (BSA; Fisher Scientific, 501613336) followed by washing three times using PBS. Subsequently, the glass slide chamber was incubated at 4 °C overnight with anti-α-syn aggregate primary antibody (Abcam, ab209538; 1:250 dilution), isotype control (Abcam, ab172730; 1:566 dilution), or vehicle. The chambers were then washed with PBS followed by an incubation with anti-goat Alexa Fluor-488 secondary antibody (Abcam, ab150077; 1:500 dilution) for 1 hour at room temperature in the dark. After washing three times, ~10 drops VECTASHEILD PLUS Antifade Mounting Medium with DAPI (Vector Laboratories, H-1900) were added to each well. All demarcation and staining steps were performed at room temperature, but the chamber slides were stored at 4 °C in the dark.

Structured illumination microscopy

Images were acquired under identical conditions using a Zeiss Elyra 7 super-resolution microscope with a x63 oil immersion lens. Images were collected using 405 nm and 488 nm laser lines for excitation; emission filters used were BP 420-480 (DAPI) and BP 495-550 (AlexaFluor 488). Sections were imaged in the absence of primary antibodies, and images were captured at the same gain as images with primary antibody. No endogenous tissue fluorescence was observed in the absence of primary antibodies. Z-stack images were obtained and processed using SIM^2 scaled to raw image. Quantification of fluorescence signal for each sample was determined by obtaining the mean intensity of the maximum intensity projection for each image given by Zen Black 3.0 software. The number of cells in each image

was counted and mean intensity per cell was calculated. For each biological sample, approximately 30-40 cells were evaluated. Background fluorescence signal was accounted for each replicate by subtracting the mean intensity per cell for the respective untreated sample. Results are expressed as arbitrary units (a.u.) of mean intensity per cell.

Data and statistical analysis

Data were plotted and statistically analyzed using GraphPad Prism 8 software. Unless stated otherwise, means ± standard error of the mean (S.E.M.) were plotted. Statistical tests performed are specified in figure legends. For all analyses, $P \le 0.05$ was considered significant. Sample sizes are noted within the main text, figure legends, and within Materials and Methods.

ASSOCIATED CONTENT

Supplementary Materials: The Supporting Information contains additional experiment details, including redox potential measurements, full dot blot membranes, comparison of antibodies for detecting aggregated α-synuclein, growth data for bacterial cultures, isotype controls for immunofluorescence microscopy experiments, and a working model of bacteria-induced dopamine-dependent α-synuclein aggregation.

AUTHOR INFORMATION

Corresponding Author: Elizabeth N. Bess, Departments of Chemistry and Molecular Biology & Biochemistry, University of California, Irvine, California, USA. E-mail: elizabeth.bess@uci.edu

Author Contributions: L.O.O. and E.N.B. developed the project. L.O.O., J.M.B., and E.N.B. designed experiments and performed data analysis. L.O.O. and J.M.B. performed experiments with contributions from K.S.U. L.O.O., J.M.B., K.S.U., and E.N.B provided critical feedback on experiments. L.O.O., J.M.B., and E.N.B. wrote the manuscript. E.N.B. acquired funds and provided project supervision and administration. All authors read and approved the final version of the manuscript.

Present Address: The current affiliation of L.O.O. is the Department of Molecular Biology and Biochemistry, University of California, Irvine, California, USA 92617.

ACKNOWLEDGMENTS

REFERENCES

(1) Braak, H.; Rüb, U.; Gai, W. P.; Del Tredici, K. Idiopathic Parkinson's Disease: Possible Routes by Which Vulnerable Neuronal Types May Be Subject to Neuroinvasion by an Unknown Pathogen. *J. Neural Transm.* **2003**, *110* (5), 517–536.

(2) Borghammer, P.; Van Den Berge, N. Brain-First versus Gut-First Parkinson's Disease: A Hypothesis. *J. Parkinsons. Dis.* **2019**, *9* (s2), S281–S295.

(3) Spillantini, M. G.; Schmidt, M. L.; Lee, V. M.; Trojanowski, J. Q.; Jakes, R.; Goedert, M. Alpha-Synuclein in Lewy Bodies. *Nature* **1997**, *388* (6645), 839–840.

(4) Chandra, R.; Hiniker, A.; Kuo, Y.-M.; Nussbaum, R. L.; Liddle, R. A. α-Synuclein in Gut Endocrine Cells and Its Implications for Parkinson's Disease. *JCI Insight* **2017**, *2* (12), e92295

(5) Paillusson, S.; Clairembault, T.; Biraud, M.; Neunlist, M.; Derkinderen, P. Activity-Dependent Secretion of Alpha-Synuclein by Enteric Neurons. *J. Neurochem.* **2013**, *125* (4), 512–517.

(6) Hilton, D.; Stephens, M.; Kirk, L.; Edwards, P.; Potter, R.; Zajicek, J.; Broughton, E.; Hagan, H.; Carroll, C. Accumulation of α-Synuclein in the Bowel of Patients in the Pre-Clinical Phase of Parkinson's Disease. *Acta Neuropathol.* **2014**, *127* (2), 235–241.

(7) Holmqvist, S.; Chutna, O.; Bousset, L.; Aldrin-Kirk, P.; Li, W.; Björklund, T.; Wang, Z.-Y.; Roybon,

L.; Melki, R.; Li, J.-Y. Direct Evidence of Parkinson Pathology Spread from the Gastrointestinal Tract to the Brain in Rats. *Acta Neuropathol.* **2014**, *128* (6), 805–820.

(8) Challis, C.; Hori, A.; Sampson, T. R.; Yoo, B. B.; Challis, R. C.; Hamilton, A. M.; Mazmanian, S. K.; Volpicelli-Daley, L. A.; Gradinaru, V. Gut-Seeded α-Synuclein Fibrils Promote Gut Dysfunction and Brain Pathology Specifically in Aged Mice. *Nat. Neurosci.* **2020**, *23* (3), 327–336.

(9) Scheperjans, F.; Aho, V.; Pereira, P. A. B.; Koskinen, K.; Paulin, L.; Pekkonen, E.; Haapaniemi, E.; Kaakkola, S.; Eerola-Rautio, J.; Pohja, M.; et al. Gut Microbiota Are Related to Parkinson's Disease and Clinical Phenotype. *Mov. Disord.* **2015**, *30* (3), 350–358.

(10) Sun, M.-F.; Shen, Y.-Q. Dysbiosis of Gut Microbiota and Microbial Metabolites in Parkinson's Disease. *Ageing Res. Rev.* **2018**, *45*, 53–61.

(11) Romano, S.; Savva, G. M.; Bedarf, J. R.; Charles, I. G.; Hildebrand, F.; Narbad, A. Meta-Analysis of the Parkinson's Disease Gut Microbiome Suggests Alterations Linked to Intestinal Inflammation. *npj Parkinson's Disease* **2021**, *7*, 27.

(12) Keshavarzian, A.; Green, S. J.; Engen, P. A.; Voigt, R. M.; Naqib, A.; Forsyth, C. B.; Mutlu, E.; Shannon, K. M. Colonic Bacterial Composition in Parkinson's Disease. *Mov. Disord.* **2015**, *30* (10), 1351–1360.

(13) Li, C.; Cui, L.; Yang, Y.; Miao, J.; Zhao, X.; Zhang, J.; Cui, G.; Zhang, Y. Gut Microbiota Differs Between Parkinson's Disease Patients and Healthy Controls in Northeast China. *Front. Mol. Neurosci.* **2019**, *12*, 171.

(14) Li, W.; Wu, X.; Hu, X.; Wang, T.; Liang, S.; Duan, Y.; Jin, F.; Qin, B. Structural Changes of Gut Microbiota in Parkinson's Disease and Its Correlation with Clinical Features. *Sci. China Life Sci.* **2017**, *60* (11), 1223–1233.

(15) Zhang, F.; Yue, L.; Fang, X.; Wang, G.; Li, C.; Sun, X.; Jia, X.; Yang, J.; Song, J.; Zhang, Y.; et al. Altered Gut Microbiota in Parkinson's Disease Patients/healthy Spouses and Its Association with Clinical Features. *Parkinsonism Relat. Disord.* **2020**, *81*, 84–88.

(16) Unger, M. M.; Spiegel, J.; Dillmann, K.-U.; Grundmann, D.; Philippeit, H.; Bürmann, J.; Faßbender, K.; Schwiertz, A.; Schäfer, K.-H. Short Chain Fatty Acids and Gut Microbiota Differ between Patients with Parkinson's Disease and Age-Matched Controls. *Parkinsonism Relat. Disord.* **2016**, *32*, 66–72.

(17) Sampson, T. R.; Debelius, J. W.; Thron, T.; Janssen, S.; Shastri, G. G.; Ilhan, Z. E.; Challis, C.; Schretter, C. E.; Rocha, S.; Gradinaru, V.; et al. Gut Microbiota Regulate Motor Deficits and Neuroinflammation in a Model of Parkinson's Disease. *Cell* **2016**, *167* (6), 1469–1480.e12.

(18) Winter, S. E.; Winter, M. G.; Xavier, M. N.; Thiennimitr, P.; Poon, V.; Keestra, A. M.; Laughlin, R. C.; Gomez, G.; Wu, J.; Lawhon, S. D.; et al. Host-Derived Nitrate Boosts Growth of E. Coli in the Inflamed Gut. *Science* **2013**, *339* (6120), 708–711.

(19) Zhu, W.; Winter, M. G.; Byndloss, M. X.; Spiga, L.; Duerkop, B. A.; Hughes, E. R.; Büttner, L.; de Lima Romão, E.; Behrendt, C. L.; Lopez, C. A.; et al. Precision Editing of the Gut Microbiota Ameliorates Colitis. *Nature* **2018**, *553* (7687), 208–211.

(20) Kishimoto, Y.; Zhu, W.; Hosoda, W.; Sen, J. M.; Mattson, M. P. Chronic Mild Gut Inflammation Accelerates Brain Neuropathology and Motor Dysfunction in α-Synuclein Mutant Mice. *Neuromolecular Med.* **2019**, *21* (3), 239–249.

(21) Grathwohl, S.; Quansah, E.; Maroof, N.; Steiner, J. A.; Spycher, L.; Benmansour, F.; Duran-Pacheco, G.; Siebourg-Polster, J.; Oroszlan-Szovik, K.; Remy, H.; et al. Specific Immune Modulation of Experimental Colitis Drives Enteric Alpha-Synuclein Accumulation and Triggers Age-Related Parkinson-like Brain Pathology. *Free Neuropathol.* **2021**, *18* (2), 2–13. https://doi.org/10.21203/rs.3.rs-100199/v1.

(22) Hare, D. J.; Double, K. L. Iron and Dopamine: A Toxic Couple. *Brain* **2016**, *139* (Pt 4), 1026–1035.

(23) Conway, K. A.; Rochet, J. C.; Bieganski, R. M.; Lansbury, P. T., Jr. Kinetic Stabilization of the Alpha-Synuclein Protofibril by a Dopamine-Alpha-Synuclein Adduct. *Science* **2001**, *294* (5545), 1346–1349.

(24) Bisaglia, M.; Mammi, S.; Bubacco, L. Kinetic and Structural Analysis of the Early Oxidation Products of Dopamine Analysis of the Interactions with α-Synuclein. *J. Biol. Chem.* **2007**, *282* (21), 15597–15605.

(25) Eisenhofer, G.; Aneman, A.; Friberg, P.; Hooper, D.; Fåndriks, L.; Lonroth, H.; Hunyady, B.;

Mezey, E. Substantial Production of Dopamine in the Human Gastrointestinal Tract. *J. Clin. Endocrinol. Metab.* **1997**, *82* (11), 3864–3871.

(26) Asano, Y.; Hiramoto, T.; Nishino, R.; Aiba, Y.; Kimura, T.; Yoshihara, K.; Koga, Y.; Sudo, N. Critical Role of Gut Microbiota in the Production of Biologically Active, Free Catecholamines in the Gut Lumen of Mice. *Am. J. Physiol. Gastrointest. Liver Physiol.* **2012**, *303* (11), G1288–G1295.

(27) Lund, E. K.; Wharf, S. G.; Fairweather-Tait, S. J.; Johnson, I. T. Increases in the Concentrations of Available Iron in Response to Dietary Iron Supplementation Are Associated with Changes in Crypt Cell Proliferation in Rat Large Intestine. *J. Nutr.* **1998**, *128* (2), 175–179.

(28) Lv, H.; Shang, P. The Significance, Trafficking and Determination of Labile Iron in Cytosol, Mitochondria and Lysosomes. *Metallomics* **2018**, *10* (7), 899–916.

(29) Radi, R. Oxygen Radicals, Nitric Oxide, and Peroxynitrite: Redox Pathways in Molecular Medicine. *Proc. Natl. Acad. Sci. U. S. A.* **2018**, *115* (23), 5839–5848.

(30) Singer, I. I.; Kawka, D. W.; Scott, S.; Weidner, J. R.; Mumford, R. A.; Riehl, T. E.; Stenson, W. F. Expression of Inducible Nitric Oxide Synthase and Nitrotyrosine in Colonic Epithelium in Inflammatory Bowel Disease. *Gastroenterology* **1996**, *111* (4), 871–885.

(31) Schöneich, C. Methionine Oxidation by Reactive Oxygen Species: Reaction Mechanisms and Relevance to Alzheimer's Disease. *Biochim. Biophys. Acta* **2005**, *1703* (2), 111–119.

(32) Balagam, B.; Richardson, D. E. The Mechanism of Carbon Dioxide Catalysis in the Hydrogen Peroxide N-Oxidation of Amines. *Inorg. Chem.* **2008**, *47* (3), 1173–1178.

(33) Circu, M. L.; Aw, T. Y. Redox Biology of the Intestine. *Free Radic. Res.* **2011**, *45* (11-12), 1245–1266.

(34) Reese, A. T.; Cho, E. H.; Klitzman, B.; Nichols, S. P.; Wisniewski, N. A.; Villa, M. M.; Durand, H. K.; Jiang, S.; Midani, F. S.; Nimmagadda, S. N.; et al. Antibiotic-Induced Changes in the Microbiota Disrupt Redox Dynamics in the Gut. *Elife* **2018**, *7*, e35987.

(35) Berg, B. L.; Stewart, V. Structural Genes for Nitrate-Inducible Formate Dehydrogenase in Escherichia Coli K-12. *Genetics* **1990**, *125* (4), 691–702.

(36) Parham, N. J.; Gibson, G. R. Microbes Involved in Dissimilatory Nitrate Reduction in the Human Large Intestine. *FEMS Microbiol. Ecol.* **2000**, *31* (1), 21–28.

(37) Carlson, H. K.; Clark, I. C.; Blazewicz, S. J.; Iavarone, A. T.; Coates, J. D. Fe(II) Oxidation Is an Innate Capability of Nitrate-Reducing Bacteria That Involves Abiotic and Biotic Reactions. *J. Bacteriol.* **2013**, *195* (14), 3260–3268.

(38) Bonnefoy, V.; Demoss, J. A. Nitrate Reductases in *Escherichia Coli*. *Antonie Van Leeuwenhoek* **1994**, *66* (1-3), 47–56.

(39) Tiso, M.; Schechter, A. N. Nitrate Reduction to Nitrite, Nitric Oxide and Ammonia by Gut Bacteria under Physiological Conditions. *PLoS One* **2015**, *10* (3), e0119712.

(40) Kortman, G. A.; Raffatellu, M.; Swinkels, D. W.; Tjalsma, H. Nutritional Iron Turned inside out: Intestinal Stress from a Gut Microbial Perspective. *FEMS Microbiol. Rev.* **2014**, *38* (6), 1202–1234.

(41) Eckburg, P. B.; Bik, E. M.; Bernstein, C. N.; Purdom, E.; Dethlefsen, L.; Sargent, M.; Gill, S. R.; Nelson, K. E.; Relman, D. A. Diversity of the Human Intestinal Microbial Flora. *Science* **2005**, *308* (5728), 1635–1638.

(42) Liu, C.-G.; Qin, J.-C.; Lin, Y.-H. Fermentation and Redox Potential. In *Fermentation Processes*; Jozala, A. F., Ed.; IntechOpen: Rijeka, 2017.

(43) Jeitner, T. M. Optimized Ferrozine-Based Assay for Dissolved Iron. *Anal. Biochem.* **2014**, *454*, 36–37.

(44) Sun, Y.; Pham, A. N.; Waite, T. D. Elucidation of the Interplay between Fe(II), Fe(III), and Dopamine with Relevance to Iron Solubilization and Reactive Oxygen Species Generation by Catecholamines. *J. Neurochem.* **2016**, *137* (6), 955–968.

(45) Abeyawardhane, D. L.; Lucas, H. R. Iron Redox Chemistry and Implications in the Parkinson's Disease Brain. *Oxid. Med. Cell. Longev.* **2019**, *2019*, 4609702.

(46) Zucca, F. A.; Segura-Aguilar, J.; Ferrari, E.; Muñoz, P.; Paris, I.; Sulzer, D.; Sarna, T.; Casella, L.; Zecca, L. Interactions of Iron, Dopamine and Neuromelanin Pathways in Brain Aging and Parkinson's Disease. *Prog. Neurobiol.* **2017**, *155*, 96–119.

(47) Munoz, P.; Huenchuguala, S.; Paris, I.; Segura-Aguilar, J. Dopamine Oxidation and Autophagy. *Parkinson's Disease* **2012**, *2012*, 920953.

(48) Paz, M. A.; Flückiger, R.; Boak, A.; Kagan, H. M.; Gallop, P. M. Specific Detection of Quinoproteins by Redox-Cycling Staining. *J. Biol. Chem.* **1991**, *266* (2), 689–692.

(49) Rothery, R. A.; Magalon, A.; Giordano, G.; Guigliarelli, B.; Blasco, F.; Weiner, J. H. The Molybdenum Cofactor of Escherichia Coli Nitrate Reductase A (NarGHI). Effect of a mobAB Mutation and Interactions with [Fe-S] Clusters. *J. Biol. Chem.* **1998**, *273* (13), 7462–7469.

(50) Habowski, A. N.; Flesher, J. L.; Bates, J. M.; Tsai, C. F.; Martin, K.; Zhao, R.; Ganesan, A. K.; Edwards, R. A.; Shi, T.; Wiley, H. S.; Shi, Y.; Hertel, K. J.; Waterman, M. L. Transcriptomic and Proteomic Signatures of Stemness and Differentiation in the Colon Crypt.. *Comms. Bio.* **2020**, *3*, 453.

(51) Bohórquez, D. V.; Shahid, R. A.; Erdmann, A.; Kreger, A. M.; Wang, Y.; Calakos, N.; Wang, F.; Liddle, R. A. Neuroepithelial Circuit Formed by Innervation of Sensory Enteroendocrine Cells. *J. Clin. Invest.* **2015**, *125* (2), 782–786.

(52) Amorim Neto, D. P.; Bosque, B. P.; Pereira de Godoy, J. V.; Rodrigues, P. V.; Meneses, D. D.; Tostes, K.; Costa Tonoli, C. C.; Faustino de Carvalho, H.; González-Billault, C.; de Castro Fonseca, M. Akkermansia Muciniphila Induces Mitochondrial Calcium Overload and α -Synuclein Aggregation in an Enteroendocrine Cell Line. *iScience* **2022**, *25* (3), 103908.

(53) Roediger, W. E.; Radcliffe, B. C. Role of Nitrite and Nitrate as a Redox Couple in the Rat Colon. Implications for Diarrheal Conditions. *Gastroenterology* **1988**, *94* (4), 915–922.

(54) McCarthy, T.; Green, B. D.; Calderwood, D.; Gillespie, A.; Cryan, J. F.; Giblin, L. STC-1 Cells. In *The Impact of Food Bioactives on Health: in vitro and ex vivo models*; Verhoeckx, K., Cotter, P., López-Expósito, I., Kleiveland, C., Lea, T., Mackie, A., Requena, T., Swiatecka, D., Wichers, H., Eds.; Springer International Publishing: Cham, 2015; pp 211–220.

(55) Friedman, E. S.; Bittinger, K.; Esipova, T. V.; Hou, L.; Chau, L.; Jiang, J.; Mesaros, C.; Lund, P. J.; Liang, X.; FitzGerald, G. A.; et al. Microbes vs. Chemistry in the Origin of the Anaerobic Gut Lumen. *Proc. Natl. Acad. Sci. U. S. A.* **2018**, *115* (16), 4170–4175.

(56) Radi, R. Oxygen Radicals, Nitric Oxide, and Peroxynitrite: Redox Pathways in Molecular Medicine. *Proc. Natl. Acad. Sci. U. S. A.* **2018**, *115* (23), 5839–5848.

(57) Conway, K. A.; Rochet, J. C.; Bieganski, R. M.; Lansbury, P. T., Jr. Kinetic Stabilization of the Alpha-Synuclein Protofibril by a Dopamine-Alpha-Synuclein Adduct. *Science* **2001**, *294* (5545), 1346–1349.

(58) Bisaglia, M.; Tosatto, L.; Munari, F.; Tessari, I.; de Laureto, P. P.; Mammi, S.; Bubacco, L. Dopamine Quinones Interact with Alpha-Synuclein to Form Unstructured Adducts. *Biochem. Biophys. Res. Commun.* **2010**, *394* (2), 424–428.

(59) Kaelberer, M. M.; Buchanan, K. L.; Klein, M. E.; Barth, B. B.; Montoya, M. M.; Shen, X.; Bohórquez, D. V. A Gut-Brain Neural Circuit for Nutrient Sensory Transduction. *Science* **2018**, *361* (6408). https://doi.org/10.1126/science.aat5236.

(60) Ye, L.; Bae, M.; Cassilly, C. D.; Jabba, S. V.; Thorpe, D. W.; Martin, A. M.; Lu, H.-Y.; Wang, J.; Thompson, J. D.; Lickwar, C. R.; et al. Enteroendocrine Cells Sense Bacterial Tryptophan Catabolites to Activate Enteric and Vagal Neuronal Pathways. *Cell Host Microbe* **2021**, *29* (2), 179–196.e9.

(61) Datsenko, K. A.; Wanner, B. L. One-Step Inactivation of Chromosomal Genes in Escherichia Coli K-12 Using PCR Products. *Proc. Natl. Acad. Sci. U. S. A.* **2000**, *97* (12), 6640–6645.

(62) Baba, T.; Ara, T.; Hasegawa, M.; Takai, Y.; Okumura, Y.; Baba, M.; Datsenko, K. A.; Tomita, M.; Wanner, B. L.; Mori, H. Construction of Escherichia Coli K-12 in-Frame, Single-Gene Knockout Mutants: The Keio Collection. *Mol. Syst. Biol.* **2006**, *2* (1), 2006.0008.

(63) Huang, C.; Ren, G.; Zhou, H.; Wang, C.-C. A New Method for Purification of Recombinant Human Alpha-Synuclein in Escherichia Coli. *Protein Expr. Purif.* **2005**, *42* (1), 173–177.

(64) Miranda, K. M.; Espey, M. G.; Wink, D. A. A Rapid, Simple Spectrophotometric Method for Simultaneous Detection of Nitrate and Nitrite. *Nitric Oxide* **2001**, *5* (1), 62–71.
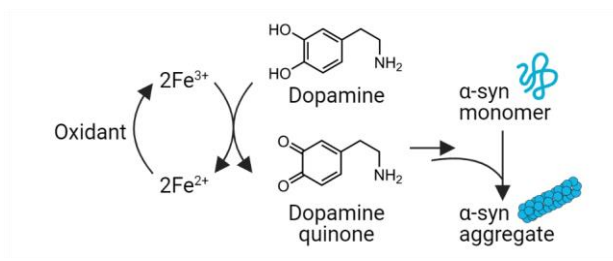
Figure 1. Upon oxidation of Fe^{2+} to Fe^{3+} in brain dopaminergic neurons, dopamine can be oxidized to *ortho*-quinones that cause α-syn to misfold and aggregate. (Figure created with BioRender.com, agreement number AA246MEBQ8.)
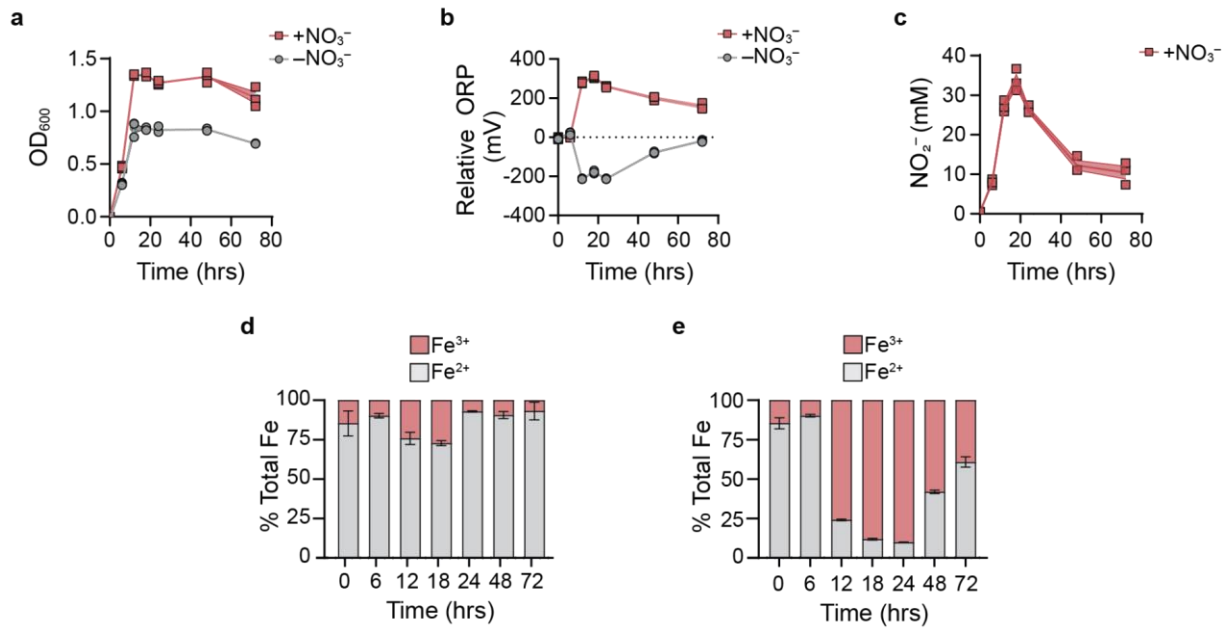
Figure 2. *E. coli* nitrate reduction generates an oxidant, nitrite, that creates an oxidizing redox potential in the bacterial environment and increases the relative abundance of Fe^{3+}. *E. coli* K-12 was incubated in mineral media with nitrate ($mM9_{+NO3}$) or without ($mM9_{-NO3}$). (a) Growth was measured by optical density at 600 nm (OD_{600}). (b) Oxidation-reduction potential (ORP) of bacterial cultures was measured, using an electrode, in culture media relative to sterile media. (c) Nitrite was quantified in cultures supplied with nitrate using the Griess assay. (d–e) Iron speciation was measured using the ferrozine assay in bacterial cultures where (d) media lacked nitrate ($mM9_{-NO3}$) or (e) media was supplemented with nitrate ($mM9_{+NO3}$). n = 3 biological replicates; bars denote means ± S.E.M.
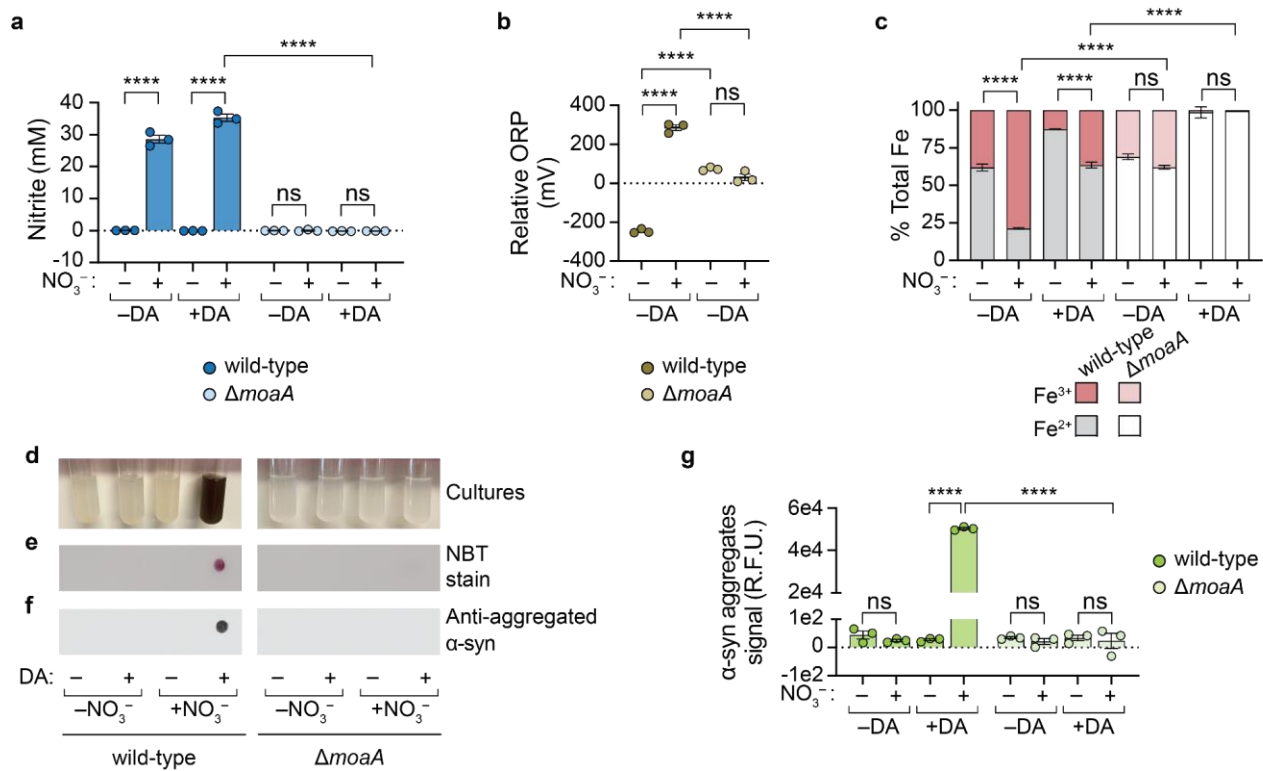
Figure 3. *E. coli* nitrate respiration instigates dopamine-dependent quinone formation and α-syn aggregation. *E. coli* K-12 wild-type or Δ*moaA* was cultured for 14 hours in mM9 media with α-syn monomer in the presence of nitrate (+NO$_3$) or its absence (-NO$_3$) and with dopamine (+DA) or without (-DA). Quantification of (a) nitrite (using Griess assay), (b) oxidation-reduction potential (ORP) relative to sterile media (using redox electrode), and (c) labile Fe^{3+} and Fe^{2+} (using ferrozine assay). (d–f) Representative images of (d) bacterial cultures as well as (e) membranes stained quinone formation (using nitroblue tetrazolium (NBT) stain) or (f) dot blots stained for α-syn aggregate formation (using immunostaining with MJFR-14 anti-fibril α-synuclein as the primary antibody). (g) Quantification of α-syn aggregates in dot blots. R.F.U.: relative fluorescence units. n = 3 biological replicates; bars denote means ± S.E.M.; significance was determined using ordinary one-way ANOVA with Sidak's multiple comparisons test; ****: $P < 0.0001$, ns: not significant.
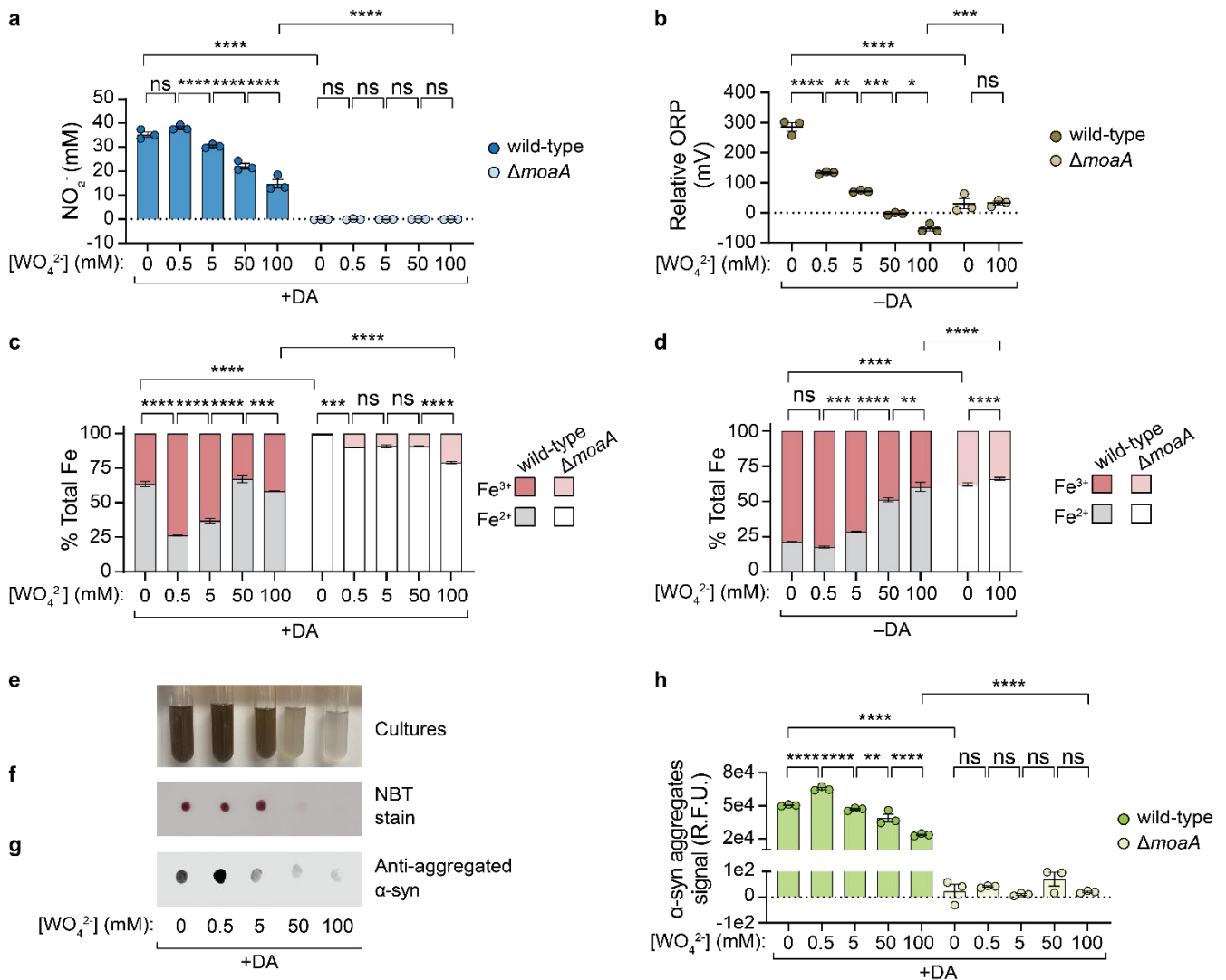
Figure 4. Tungstate limits α-syn aggregation by inhibiting bacterial nitrate reduction, which reduces redox potential of the bacterial environment. *E. coli* K-12 wild-type or Δ*moaA* was cultured for 14 hours in mM9 media with α-syn monomer in the presence of nitrate ($+NO_3$), with dopamine (+DA) or without (-DA), and with sodium tungstate (WO_4^{2-}) at varying concentrations (0–100 mM). Quantification of (a) nitrite (using Griess assay), (b) oxidation-reduction potential (ORP) relative to sterile media (using redox electrode), and (c–d) labile Fe^{3+} and Fe^{2+} (using ferrozine assay) in cultures (c) with dopamine or (d) without dopamine. (e–g) Representative images of (e) bacterial cultures of *E. coli* K-12 wild-type incubated in $mM9_{+NO3, +DA}$ supplemented with tungstate (0–100 mM) as well as (f) membranes stained for quinone formation (using nitroblue tetrazolium (NBT) stain) or (g) dot blots stained for α-syn aggregate formation (using immunostaining with MJFR-14 anti-fibril α-synuclein as the primary antibody). (h) Quantification of α-syn aggregates in dot blots. R.F.U.: relative fluorescence units. n = 3 biological replicates; bars denote means ± S.E.M.; significance was determined using ordinary one-way ANOVA with Sidak's multiple comparisons test; ****: $P < 0.0001$, ***: $P < 0.0007$, **: $P < 0.0026$, *: $P = 0.0168$, ns: not significant.
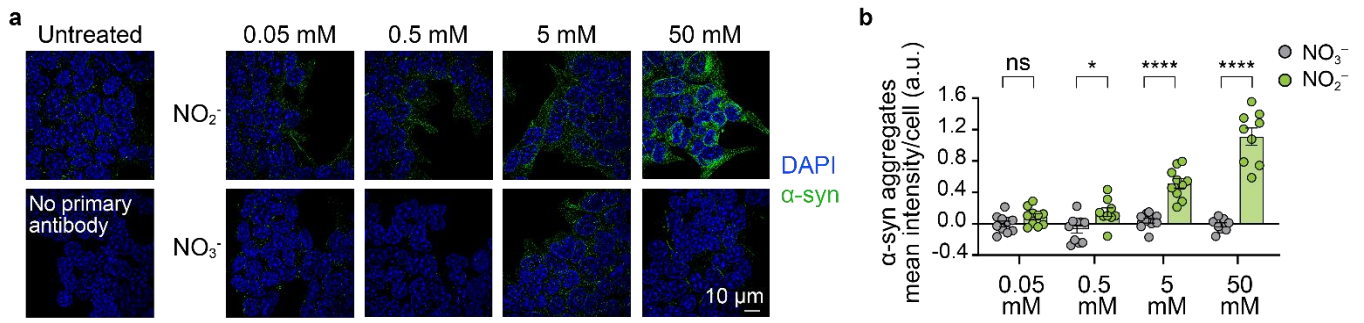
Figure 5. Nitrite, but not nitrate, induces α-syn aggregation in enteroendocrine STC-1 cells. α-Syn aggregates per STC-1 cell upon incubation with nitrate (NO_3^-) or nitrite (NO_2^-) were (a) visualized (representative images) and (b) quantified using maximum intensity projections acquired by structured illumination microscopy (immunofluorescence staining of α-syn aggregates is in green; DAPI-stained cell nuclei are in blue). n = 3 independent biological replicates, 3–4 technical replicates for each; bars denote mean ± S.E.M.; significance determined by unpaired t-test; *: $P = 0.0113$; ****: $P < 0.0001$, ns: not significant.

Table of Contents Graphic: